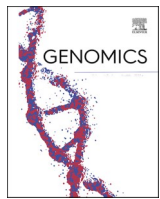
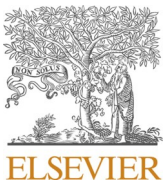




Since January 2020 Elsevier has created a COVID-19 resource centre with free information in English and Mandarin on the novel coronavirus COVID-19. The COVID-19 resource centre is hosted on Elsevier Connect, the company's public news and information website.

Elsevier hereby grants permission to make all its COVID-19-related research that is available on the COVID-19 resource centre - including this research content - immediately available in PubMed Central and other publicly funded repositories, such as the WHO COVID database with rights for unrestricted research re-use and analyses in any form or by any means with acknowledgement of the original source. These permissions are granted for free by Elsevier for as long as the COVID-19 resource centre remains active.



Original Article

Vaccine-escape and fast-growing mutations in the United Kingdom, the United States, Singapore, Spain, India, and other COVID-19-devastated countries

Rui Wang ^a, Jiahui Chen ^a, Kaifu Gao ^a, Guo-Wei Wei ^{a,b,c,*}^a Department of Mathematics, Michigan State University, MI 48824, USA^b Department of Electrical and Computer Engineering, Michigan State University, MI 48824, USA^c Department of Biochemistry and Molecular Biology, Michigan State University, MI 48824, USA

ARTICLE INFO

ABSTRACT

Keywords:
 COVID-19
 SARS-CoV-2
 Mutation
 Vaccine escape
 Antibody
 Binding affinity
 Persistent homology
 Deep learning

Recently, the SARS-CoV-2 variants from the United Kingdom (UK), South Africa, and Brazil have received much attention for their increased infectivity, potentially high virulence, and possible threats to existing vaccines and antibody therapies. The question remains if there are other more infectious variants transmitted around the world. We carry out a large-scale study of 506,768 SARS-CoV-2 genome isolates from patients to identify many other rapidly growing mutations on the spike (S) protein receptor-binding domain (RBD). We reveal that essentially all 100 most observed mutations strengthen the binding between the RBD and the host angiotensin-converting enzyme 2 (ACE2), indicating the virus evolves toward more infectious variants. In particular, we discover new fast-growing RBD mutations N439K, S477N, S477R, and N501T that also enhance the RBD and ACE2 binding. We further unveil that mutation N501Y involved in United Kingdom (UK), South Africa, and Brazil variants may moderately weaken the binding between the RBD and many known antibodies, while mutations E484K and K417N found in South Africa and Brazilian variants, L452R and E484Q found in India variants, can potentially disrupt the binding between the RBD and many known antibodies. Among these RBD mutations, L452R is also now known as part of the California variant B.1.427. Finally, we hypothesize that RBD mutations that can simultaneously make SARS-CoV-2 more infectious and disrupt the existing antibodies, called vaccine escape mutations, will pose an imminent threat to the current crop of vaccines. A list of most likely vaccine escape mutations is given, including S494P, Q493L, K417N, F490S, F486L, R403K, E484K, L452R, K417T, F490L, E484Q, and A475S. Mutation T478K appears to make the Mexico variant B.1.1.222 the most infectious one. Our comprehensive genetic analysis and protein-protein binding study show that the genetic evolution of SARS-CoV-2 on the RBD, which may be regulated by host gene editing, viral proofreading, random genetic drift, and natural selection, gives rise to more infectious variants that will potentially compromise existing vaccines and antibody therapies.

1. Introduction

Up to April 18, 2021, coronavirus disease 2019 (COVID-19) caused by severe acute respiratory syndrome coronavirus 2 (SARS-CoV-2) has taken 3,004,842 lives and infected 140,373,125 people according to the data from World Health Organization (WHO). The first complete SARS-CoV-2 genome sequence was deposited to the GenBank (Access number: NC_045512.2) on January 5, 2020. Thereafter, new SARS-CoV-2 genome sequences were accumulated rapidly at the GenBank and GISAID, which laid the foundations for analyzing the SARS-CoV-2 mutations, virulence,

pathogenicity, antigenicity, and transmissibility. A complete SARS-CoV-2 genome is an unsegmented positive-sense single-stranded RNA virus, which encodes 29 structural and non-structural proteins (NSPs) by its 29,903 nucleotides. NSPs play vital roles in RNA replication, while structural proteins form the viral particle. There are four structural proteins on SARS-CoV-2, namely, spike (S), envelope (E), membrane (M), and nucleocapsid (N) proteins [1–4]. Among them, the S protein with 1273 residues of SARS-CoV-2 has drawn much attention due to its critical role in viral infection and the development of vaccines and antibody drugs.

* Corresponding author at: Department of Mathematics, Michigan State University, MI 48824, USA.

E-mail address: weig@msu.edu (G.-W. Wei).

The SARS-CoV-2 enters the host cell by interacting between its S protein and the host angiotensin-converting enzyme 2 (ACE2), primed by host transmembrane protease, serine 2 (TMPRSS2) [5]. Such a process initiates the response from the host adaptive immune system, which generates antibodies to combat the invading virus. Therefore, the S protein of SARS-CoV-2 has become a target in the development of antibody therapies and vaccines. A major concern is the potential impacts of S protein mutations on viral infectivity, the existing vaccines, and antibody therapies.

The most well-known mechanism of mutations is the random genetic drift, which plays a role in the processes of transcription, translation, replication, etc. Compared with DNA viruses, RNA viruses are more prone to random mutations. Unlike other RNA viruses, such as influenza, SARS-CoV-2 has a genetic proofreading mechanism regulated by NSP14 and NSP12 (a.k.a RNA-dependent RNA polymerase) [6,7], which enables SARS-CoV-2 to have a higher fidelity in its replication. However, the host gene editing has been found to be the major source for existing SARS-CoV-2 mutations [8], counting for 65% of reported mutations. Therefore, the worldwide transmission of COVID-19 provides SARS-CoV-2 an abundant opportunity to experience fast mutations. Another important mechanism for SARS-CoV-2 evolution is natural selection, which makes the virus more infectious while less virulent, in general [9,10].

It has been established that the infectivity of different viral variants in host cells is proportional to the binding free energy (BFE) between the RBD of each variant and the ACE2 [5,11–14]. Based on such a principle, it has been reported that mutations on the S protein have strengthened SARS-CoV-2 infectivity [15]. Whereas, virulent can be due to mutations on many SARS-CoV-2 proteins. The widely spread asymptomatic COVID-19 infection and transmission can be a result of mutation-induced virulent changes [16].

Recently, the United Kingdom (UK) variant B.1.1.7 (a.k.a 20I/501Y.V1) [17], the South Africa variant B.1.351 (a.k.a 20H/501Y.V2) [18], the Brazil(ian) variant P.1 (a.k.a 20J/501Y.V3) [19], and the India variant B.1.617 [20] have been circulating worldwide, including the United States (US) and Spain. These variants contain mutations on the S protein RBD and are widely speculated to make SARS-CoV-2 more infectious. Specifically, all three variants involve RBD mutation N501Y, whereas the South Africa and Brazil(ian) variants also contain RBD mutations E484K and K417N.

An important question is how these new variants will affect the vaccines and antibody drugs. Ideally, this question should be answered by experiments. However, SARS-CoV-2 has more than 28,000 unique single mutations, with nearly 7000 of them on the S protein, which are intractable for experimental means. In May 2020, an intensively validated topology-based neural network tree (TopNetTree) model [21] was employed to predict certain RBD mutations, including E484K, L452R, and K417N, would strengthen SARS-CoV-2 infectivity [15]. These predictions have been confirmed [17–19]. Additionally, all 451 new RBD mutations occurred since May 2020 were predicted as the most likely mutations in our work published online last May [15]. We also predicted a list of 625 unlikely RBD mutations [15] and currently, none of them has ever been observed. Recently, our TopNetTree model has been trained on SARS-CoV-2 datasets to accurately predict the S protein and ACE2 or antibody binding free energy changes induced by mutations [22]. A total of 31 disruptive mutations on S protein RBD has been reported as the potential mutations that would most likely disrupt the binding of S protein and essentially all the known SARS-CoV-2 antibodies had they ever occurred [22]. Therefore, tracking the growth rate of existing mutations on S protein RBD enables us to monitor the mutations that may impact the efficacy of the existing vaccines and antibody drugs. The study of fast-growing mutations also enables us to understand the SARS-CoV-2 evolutionary tendency and eventually predict future mutations.

The objective of this work is to track the fast-growing RBD mutations in pandemic-devastated countries and to analyze its evolutionary

tendency around the world based on one of the most comprehensive data sets involving 506,768 SARS-CoV-2 genome sequences shown in the Mutation Tracker (https://users.math.msu.edu/users/weig/SARS-CoV-2_Mutation_Tracker.html). We found 6945 unique single mutations on the S protein and among them, 1024 occurred on the RBD. In terms of protein sequence, 100 of 651 non-degenerate mutations on the RBD were observed more than 28 times in the database and are regarded as significant mutations. We show that in addition to mutations N501Y, E484K, and K417N in the UK, South Africa, and Brazil(ian) variants, L452R, E484Q in the India variants, N439K, S477N, S477R, and N501T are also fast-growing mutations in 31 pandemic-devastated countries in the past few months. Using the TopNetTree model [21,22], we discover that essentially all 100 most observed mutations on the RBD are associated with the BFE strengthening of the binding of the RBD and ACE2 complex, resulting in more infectious SARS-CoV-2 variants. Considering mutation occurrence probability and ability to disrupt antibodies, we identify vaccine-escape and vaccine-weakening RBD mutations. The present finding suggests that S protein RBD mutations, in general, make the virus more infectious and are disruptive to the existing vaccines and antibody drugs.

2. Results

2.1. Gene-specific analysis on the S protein and the RBD

Driven by natural selection, random genetic drift, gene editing, host immune responses, etc. [9,10], viruses constantly evolve through mutations, which create genetic diversity and generates new variants. To have a good understanding of how the mutation will affect the infectivity, transmission, and virulence of SARS-CoV-2, it will be of great importance to study the mutations on SARS-CoV-2, particularly the S protein and its RBD, over a long time period. Therefore, in this work, we mainly focus on the mutations in S protein and S protein RBD. Here, a total of 28,507 unique single mutations has been decoded from 651,768 complete SARS-CoV-2 genome sequences.

Table 1 shows the distribution of 12 single-nucleotide polymorphism (SNP) types among 6945 unique mutations and 2,194,305 non-unique mutations on the S gene of SARS-CoV-2 worldwide. Symbols N_U , N_{NU} , R_U , and R_{NU} represent the number of unique mutations, the number of non-unique mutations, the ratio of 12 SNP types among unique mutation, and the ratio of 12 SNP types among non-unique mutations, respectively. It can be seen that A>G and C>T have a higher ratio in unique and non-unique cases, which may be related to the host immune response via APOBEC and ADAR gene editing as reported in [8]. Moreover, T>C has the highest mutation ratios among unique mutations. However, the ratio of T>C mutations among the non-unique mutations is not very high, indicating that T>C mutations do not commonly occur in the population.

Table 2 shows the distribution of 12 SNP types among 1024 unique mutations and 266,458 non-unique mutations on the spike RBD gene sequence of SARS-CoV-2 worldwide. To be noticed, compared to **Table 1**, the distribution of 12 SNP types acts differently on S protein RBD. The top 3 highest mutation ratios among non-unique mutations are A>T, G>A, and C>A, which indicating that these 3 types of mutations may have a higher impact on the transmission of SARS-CoV-2.

Fig. 1 is the 2D amino acid sequence alignment for the S protein RBD of SARS-CoV-2, Bat-SL-RaTG13, Pangolin-CoV, SARS-CoV, and Bat-SL-BM48-31. It can be seen that residues R346, N354, K417, N438, N440, S443, K444, V445, K458, N460, T478, S494, Q495, and Q498 located on the S protein RBD is not conservative, while the other residues are relatively conservative among different species.

2.2. Impacts of SARS-CoV-2 spike RBD mutations on SARS-CoV-2 infectivity

The RBD is located on the S1 domain of the S protein, which plays a

Table 1

The distribution of 12 SNP types among 6945 unique mutations and 2,194,305 non-unique mutations on the S gene of SARS-CoV-2 worldwide. N_U is the number of unique mutations and N_{NU} is the number of non-unique mutations. R_U and R_{NU} represent the ratios of 12 SNP types among unique and non-unique mutations. In this table, we bold the ratios that are greater than 10%.

SNP type	Mutation type	N_U	N_{NU}	R_U	R_{NU}	SNP type	Mutation type	N_U	N_{NU}	R_U	R_{NU}
A>T	Transversion	655	187,467	9.43%	8.54%	C>T	Transition	609	488,323	8.77%	22.25%
A>C	Transversion	567	12,914	8.16%	0.59%	C>A	Transversion	466	369,637	6.71%	16.85%
A>G	Transition	908	530,814	13.07%	24.19%	C>G	Transversion	269	3965	3.87%	0.18%
T>A	Transversion	589	6690	8.48%	0.30%	G>T	Transversion	523	111,949	7.53%	5.10%
T>C	Transition	976	60,918	14.05%	2.78%	G>C	Transversion	342	182,984	4.92%	8.34%
T>G	Transversion	498	179,748	7.17%	8.19%	G>A	Transition	543	58,896	7.82%	2.68%

Table 2

The distribution of 12 SNP types among 1024 unique mutations and 266,458 non-unique mutations on the spike RBD gene of SARS-CoV-2 worldwide. N_U is the number of unique mutations and N_{NU} is the number of non-unique mutations. R_U and R_{NU} represent the ratios of 12 SNP types among unique and non-unique mutations. In this table, we bold the ratios that are greater than 10%.

SNP type	Mutation type	N_U	N_{NU}	R_U	R_{NU}	SNP type	Mutation type	N_U	N_{NU}	R_U	R_{NU}
A>T	Transversion	84	170,165	8.20%	63.86%	C>T	Transition	90	11,562	8.79%	4.34%
A>C	Transversion	75	3685	7.32%	1.38%	C>A	Transversion	66	16,551	6.45%	6.21%
A>G	Transition	134	2310	13.09%	0.87%	C>G	Transversion	38	694	3.71%	0.26%
T>A	Transversion	89	890	8.69%	0.33%	G>T	Transversion	79	7419	7.71%	2.78%
T>C	Transition	161	7308	15.72%	2.74%	G>C	Transversion	47	907	4.59%	0.34%
T>G	Transversion	76	11,318	7.42%	4.25%	G>A	Transition	85	33,649	8.30%	12.63%

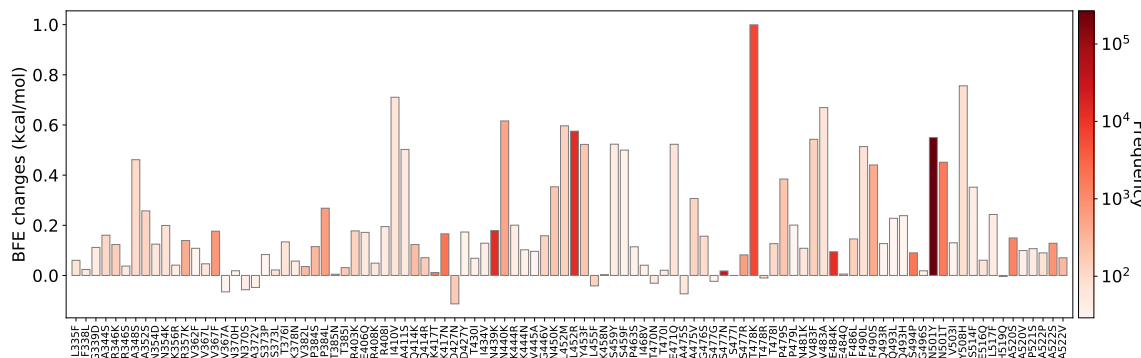
SARS-CoV-2 329 **F** P N I T N L C P F G E V F N A T R F A S V Y A W R K R I S N C V A D Y S V L Y N S A S F S T F K C Y G V S P T K L N D L C F T N V Y A D S F V I R G D E V R Q I A P G Q T G K I A D Y N Y K L P D D F 429
SARS-CoV 316 **F** P N I T N L C P F G E V F N A T K F P S V Y A W E R K K I S N C V A D Y S V L Y N S T F F S T F K C Y G V S A T K L N D L C F S N V Y A D S F V V K G D D V R Q I A P G Q T G V I A D Y N Y K L P D D F 416
Bat-SL-RaTG13 329 **F** P N I T N L C P F G E V F N A T T F A S V Y A W W R K R I S N C V A D Y S V L Y N S T S F S T F K C Y G V S P T K L N D L C F T N V Y A D S F V I T G D E V R Q I A P G Q T G K I A D Y N Y K L P D D F 429
Bat-SL-BM48-31 320 **F** P N I T Q L C P F N E V F N I T S F P S V Y A W E R M R I T N C V A D Y S V L Y N S A S F S T F C C Y G V S P T K L N D L C F S V S V Y A D Y F V V V K G D D V R Q I A P Q T G V I A D Y N Y K L P D D F 421
Pangolin-CoV 329 **F** P N I T N L C P F G E V F N A S K F A S V Y A W W R K R I S N C V A D Y S V L Y N S T S F S T F K C Y G V S P T K L N D L C F T N V Y A D S F V V K G D E V R Q I A P G Q T G V I A D Y N Y K L P D D F 429

SARS-CoV-2 430 **G** C V I A W V N S N N L D S K V G G N Y N Y L Y R L F R K S N L K P F E R D I S T E I Y Q A G S T P C N G V E G F N C Y F P L Q S Y G F Q P T N G V G Y Q P Y R V V V L S F E L L H A P A T V C G P K K S 530
SARS-CoV 417 M G C V L A W V N T R N I D A T S T G N Y N Y K Y R Y R L H G K L R P F E R D I S N V P S P D G K P C T - P P A L N C Y W P L N D Y G F Y T T T G I G Y Q P Y R V V V L S F E L L N A P A T V C G P K L S 516
Bat-SL-RaTG13 430 **G** C V I A W V N S K H I D A K E G G N F N Y L Y R L F R K S N L K P F E R D I S T E I Y Q A G S K P C N G Q T G L N C Y P L Y R G Y P T D G V H Q P Y R V V V L S F E L L N A P A T V C G P K K S 530
Bat-SL-BM48-31 422 **G** C V I A W V N T S L D S S N - - - E F F Y R R F R H G K I K P Y G R D L S N V L F N P S G G T C S - A E G L N C Y K P L A S Y G F T Q S S G I G F Q P Y R V V V L S F E L L N A P A T V C G P K Q S 517
Pangolin-CoV 430 **G** C V I A W V N S V K Q D A L T G G N Y G Y L Y R L F R K S N L K P F E R D I S T E I Y Q A G S T P C N G Q V G L N C Y Y P L E R Y G F H P T T G V N Y Q P F R V V V L S E L L N G P A T V C G P K L S 530

Fig. 1. 2D sequence alignment for the S protein RBD of SARS-CoV-2, Bat-SL-RaTG13, Pangolin-CoV, SARS-CoV, and Bat-SL-BM48-31.

vital role in binding with the human ACE2 to get entry into host cells. The mutations that are detected on the RBD may affect the binding process and lead to the BFE changes. In this section, we apply the TopNetTree model [22] to predict the mutation-induced BFE changes of RBD and ACE2. Fig. 2 illustrates the predicted BFE changes for S protein and human ACE2 induced by single-site mutations on the RBD. Here, we consider 100 most observed mutations. The bar plot of the other mutations on S RBD can be found in the Supporting Information. In this figure, a total of 100 most observed mutations are displayed. Among them, 9 mutations induce negligible negative BFE changes, while the other 91 mutations are binding-strengthening mutations. Mutation T478K has the largest BFE change which is nearly 1 kcal/mol. It may have made the Mexico variant B.1.1.222 the most infectious observed variant. To be noted, the residue T478 is not conservative among

different species as illustrated in Fig. 1. The N501Y, S477N, L452R, N439K, and E484K mutations are the top mutations with significant frequencies. Among them, the N501Y and L452R mutations have relatively high BFE changes of 0.55 kcal/mol and 0.58 kcal/mol, respectively. Moreover, the frequency and predicted BFE changes are both at a high level for mutations N501T, Y508H. Fig. 3 illustrates the time evolution of 651 binding-strengthening (blue) and binding-weakening mutations (red) on the S protein RBD. Here, the y-axis reveals the natural log frequency of each mutation. Based on our previous findings in [15], at this stage, 651 out of 1149 RBD mutations that we predicted as “most likely” mutations have been observed, and none of the 1912 “likely” and 625 “unlikely” mutations are tracked on the S protein RBD, suggesting the reliability of our model for predicting the BFE changes of S protein RBD and ACE2. Among 651 mutations that are detected on

**Fig. 2.** Illustration of SARS-CoV-2 mutation-induced BFE changes for the complexes of S protein and ACE2. Here, 100 most observed mutations on S RBD are illustrated.

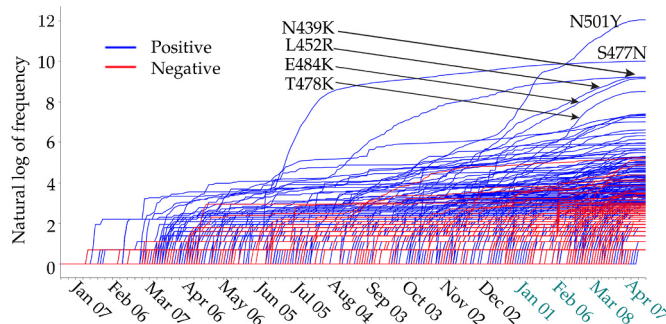


Fig. 3. Illustration of the time evolution of 424 ACE2 binding-strengthening RBD mutations (blue) and 227 ACE2 binding-weakening RBD mutations (red) on the S protein RBD of SARS-CoV-2 from Jan 07, 2020 to April 18, 2021. The x-axis represents date and y-axis represents the natural log of frequency of each mutation. (For interpretation of the references to colour in this figure legend, the reader is referred to the web version of this article.)

RBD, mutations N501Y, S477N, L452R, N439K, and E484K have the highest frequency up to April 18, 2021.

It is important to those mutations that have been recorded with high frequency the beginning of 2021. Table 3 gives such information for top 40 mutations in 2021. It can be seen that mutations N501Y, L452R, T478K, N501T, N550K, F490S, V483F, L452M, and A348S have relatively high BFE changes of the binding of S protein and ACE2, suggesting that they may lead to more infectious variants.

Fig. 4 shows the 3D structure of SARS-CoV-2 S protein RBD bound with ACE2. Here, we mark 13 mutations with either high frequency or high BFE changes. The blue and red colors represent the mutations that have positive and negative BFE changes, respectively. The darker the colour is, the larger the absolute value of the BFE change is. While mutations occur everywhere on the spike protein, the ones that are most important to COVID-19 infectivity and the efficacy of antibodies and vaccines are located at the interface between the spike protein and ACE2 or antibodies.

2.3. Impacts of SARS-CoV-2 spike RBD mutations on COVID-19 vaccines

It is of paramount importance to track not only ACE2-binding-strengthening RBD mutations and FG mutations but also the antibody-binding-weakening RBD mutations. Our early work reported nearly 71% mutations on the S protein RBD will weaken the binding of S

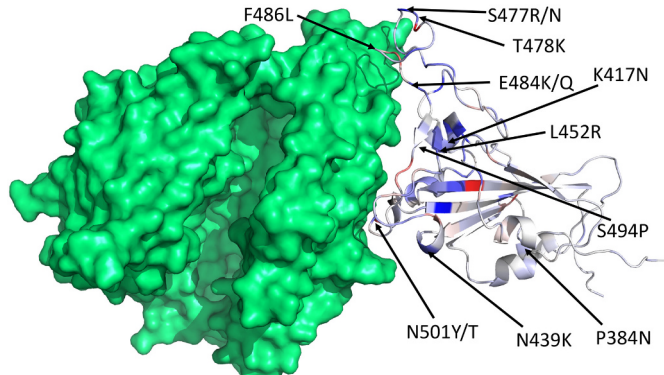


Fig. 4. The 3D structure of SARS-CoV-2 S protein RBD bound with ACE2 (PDB ID: 6M0J). We choose blue and red colors to mark the binding-strengthening and binding-weakening mutations, respectively. Vaccine escape mutations described in Table 4 are labeled. (For interpretation of the references to colour in this figure legend, the reader is referred to the web version of this article.)

protein and antibodies, while 64.9% mutations on the RBD will strengthen the binding of S protein and ACE2, suggesting that these mutations may potentially enhance the infectivity of SARS-CoV-2 and make the existing antibodies less effective [22]. We call those mutations that weaken the binding of the S protein and most SARS-CoV-2 antibodies as antibody disrupting (AD) mutations [22]. Notably, most antibody disrupting mutations have negative BFE changes, suggesting that they will make the SARS-CoV-2 less infectious and thus, will not frequently occur due to natural selection. As a result, many of them may not be able to evade the existing vaccines in a population. Therefore, it is necessary to focus on the BFE changes of S protein and antibodies that are induced by 100 most observed mutations on S protein RBD.

In this work, we have collected a total of 106 antibodies. The detailed information of these 106 antibodies can be found in the Supporting Information. Fig. 5 shows the BFE changes for the S protein and 106 antibody complexes together with ACE2 following 100 most observed mutations on the S protein RBD. The red colour marks the mutation-induced negative BFE changes for the complexes of S protein and antibodies, which indicates that these mutations may weaken the binding and make the antibody less effective. Meanwhile, the green colour represents the positive BFE changes induced by mutations, which suggests that these mutations may strengthen the binding between S protein and antibodies. From Fig. 5, we can see that mutation E484K will

Table 3

List of top 40 high-frequency (HF) mutations and their corresponding BFE changes (unit: kcal/mol) of the binding of S protein and ACE2. Here, count shows the frequency occurred in 2021.

Rank	HF mutation	Count	BFE change	Rank	HF mutation	Count	BFE change
Top 1	N501Y	168,801	0.5499	Top 21	N450K	184	0.3535
Top 2	L452R	9843	0.5752	Top 22	E484Q	182	0.0057
Top 3	E484K	9350	0.0946	Top 23	P330S	182	0.0533
Top 4	S477N	9276	0.018	Top 24	A522V	179	0.0705
Top 5	N439K	6056	0.1792	Top 25	D427N	164	-0.1133
Top 6	T478K	4935	0.9994	Top 26	P479S	153	0.3844
Top 7	K417N	1634	0.1661	Top 27	V382L	151	0.0355
Top 8	K417T	1508	0.0116	Top 28	T385N	151	0.0049
Top 9	S494P	1483	0.0902	Top 29	Q414R	143	0.0708
Top 10	N501T	1295	0.4514	Top 30	R346K	135	0.1234
Top 11	A520S	819	0.1495	Top 31	T385I	127	0.0314
Top 12	A522S	621	0.1283	Top 32	R403K	121	0.1778
Top 13	V367F	536	0.1764	Top 33	L455F	99	-0.0415
Top 14	N440K	432	0.6161	Top 34	V483F	99	0.5428
Top 15	S477R	394	0.082	Top 35	A475V	96	0.3069
Top 16	P384L	389	0.2681	Top 36	G446V	86	0.1583
Top 17	R357K	373	0.1393	Top 37	L452M	83	0.5966
Top 18	F490S	363	0.4406	Top 38	A348S	82	0.4616
Top 19	P384S	263	0.1151	Top 39	T478I	81	0.1269
Top 20	Q414K	224	0.1234	Top 40	A352S	78	0.2576

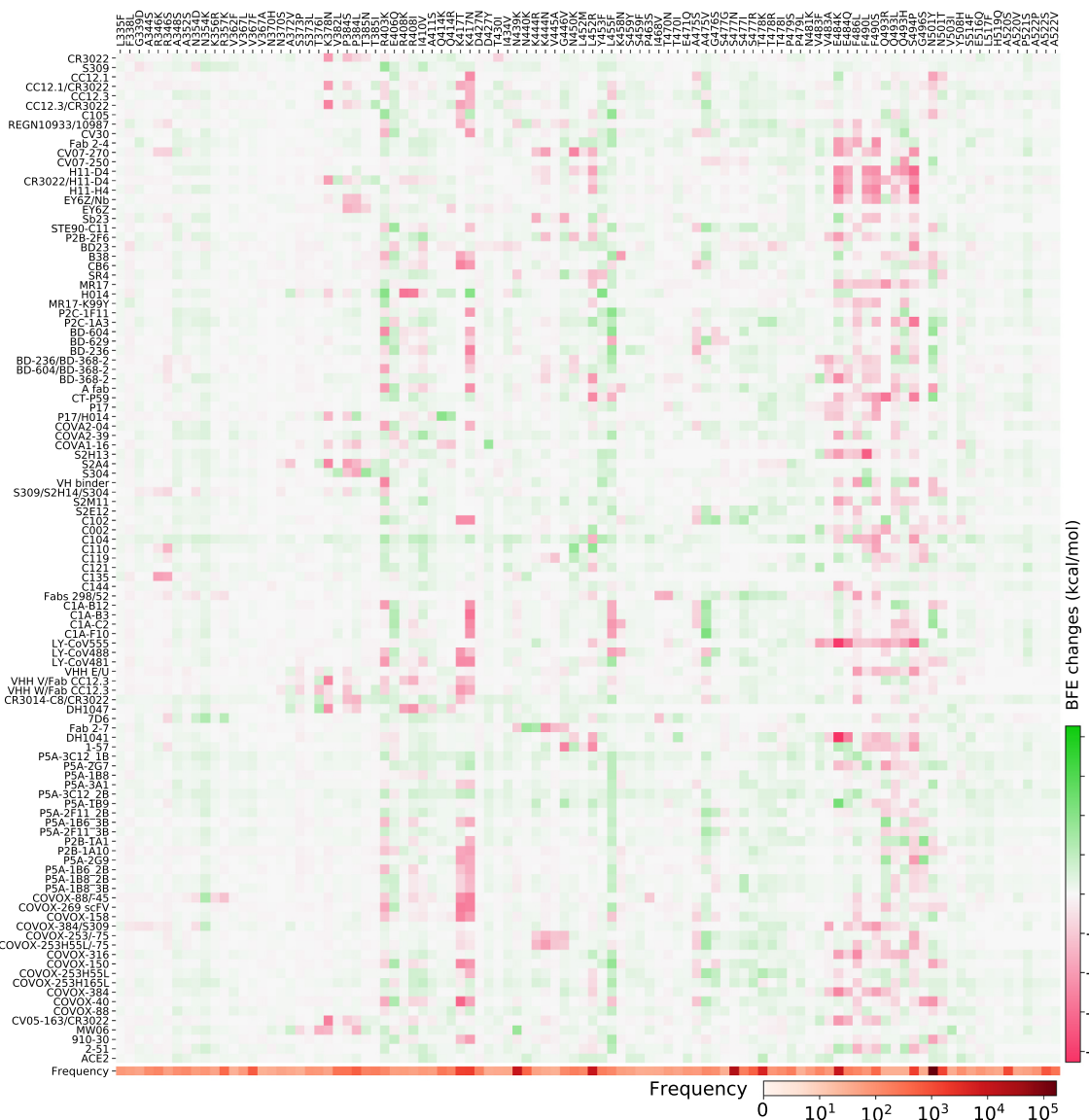


Fig. 5. Illustration of SARS-CoV-2 S RBD 100 most observed mutations induced BFE changes for the complexes of S protein and 106 antibodies or ACE2. Here, red colour represents the negative changes that will weaken the binding, while the green colour shows the positive changes that will strengthen the binding. (For interpretation of the references to colour in this figure legend, the reader is referred to the web version of this article.)

disruptively weaken the binding of S protein with antibodies such as LY-CoV555 and DH1041, which are marked in dark red. Mutation S494P will disruptively weaken the binding of S protein with antibodies such as H11-D4, H11-H4, and LY-CoV555. Mutation K417N will disruptively weaken the binding of S protein with a large number of antibodies. Moreover, mutation N501Y will moderately weaken the binding of S protein with antibodies such as CC12.1/CR3022, COVOX-88/-45, COVOX-88, etc.

Considering the impact of the possible calculation error, we set -0.3 kcal/mol as the threshold of the binding between S protein and antibodies induced by AD mutations. Specifically, we say a mutation is an AD mutation to the binding complex of S protein and antibody if its BFE change for the complex is less than 0.3 kcal/mol. We hypothesize that RBD mutations that can simultaneously strengthen the infectivity and disrupt the binding between the S protein and existing antibodies will pose imminent threats to the current crop of vaccines. We define a vaccine escape (VE) mutation as a high-frequency mutation that is an AD mutation for at least 24 (23%) different antibodies. We also define a vaccine-weakening (VW) mutation as a high-frequency mutation and AD mutation for 11 (10%) to 21 (20%) different antibodies.

Table 4

List of vaccine escape (VE) and vaccine weakening (VW) Their corresponding BFE changes (unit: kcal/mol) of the binding of S protein and ACE2 are provided as well. Here, the count shows the number of antibodies that will make a specific mutation to be an AD mutation.

VE mutation	BFE change	Count	VW mutation	BFE change	Count
S494P	0.0902	50	N501Y	0.5499	21
Q493L	0.2279	43	Q493R	0.1271	21
K417N	0.1661	43	R408I	0.1949	19
F490S	0.4406	42	Q493H	0.2385	18
F486L	0.1456	41	P384S	0.1151	18
R403K	0.1778	34	K378N	0.0573	16
E484K	0.0946	31	G496S	0.0187	15
L452R	0.5752	28	L455F	-0.0415	15
K417T	0.0116	28	I410V	0.7105	14
F490L	0.5139	25	R346S	0.0374	14
E484Q	0.0057	25	V483A	0.6695	13
A475S	-0.0732	24	K444N	0.1024	12
			N501T	0.4514	11
			P384L	0.2681	11

Table 4 lists vaccine-escape (VE) and vaccine-weakening (VW) RBD mutations together with their corresponding BFE changes (unit: kcal/mol) of the binding between S protein and ACE2. The count represents the number of antibodies that will make a specific mutation to be an AD mutation. We can see that VE mutations F490S, L452R, VW mutations F490L, N501Y, V483A, and N501T have relatively high BFE changes of the binding of S protein and ACE2, suggesting that they are high-risk mutations. Moreover, L452R, N501Y, and N501T are also HF mutations, which should receive high attention.

2.4. Fast-growing mutations in COVID-19-devastated countries

In this section, we extract the 31 countries with the highest number of SNP profiles and analyze their mutations on S protein RBD, as illustrated in **Table 5**. We can see that the BFE changes of S protein and ACE2 induced by mutations on the RBD are mostly positive, suggesting that the binding between ACE2 and S protein will be potentially strengthened in these 31 countries. This indicates that SARS-CoV-2 becomes more infectious, driven by most mutations on the receptor-binding domain.

Tracking the binding-strengthening mutations will play a vital role in the development of anti-virus drugs, antibody drugs, and vaccines. Therefore, we calculate the growth rate of mutations on the RBD on a 10-day average, aiming to monitor the binding-strengthening mutations that have rapid growth over time. **Fig. 6** illustrates the log growth rate and log frequency of mutations on the S protein RBD in the United Kingdom on a 10-day average. The blue and red colors respectively represent the positive and negative BFE changes induced by a specific mutation, and the purple colour represents the log frequency of a specific mutation. The darker the colour is, the higher the log growth rate/

Table 5

The statistical analysis of mutations on S protein RBD of 31 countries with large sequencing data. N_{seq} is the number of sequences in each country. N_{U-RBD} is the number of unique mutations on RBD and N_{NU-RBD} is the number of non-unique mutations on RBD. $N_{positive}$ and $N_{negative}$ represent the number of unique single mutations that will respectively result in positive and negative BFE changes of S protein and ACE2 induced by mutations on S protein RBD.

Country (Country code)	N_{seq}	N_U	N_{NU}	$N_{positive}$	$N_{negative}$
United Kingdom (UK)	174,372	297	98,015	234	63
United States (USA)	127,809	352	44,660	252	100
Denmark (DK)	29,689	94	9628	81	13
Germany (DE)	18,778	324	16,033	207	117
Canada (CA)	13,050	64	1180	55	9
Netherlands (NL)	12,293	86	7824	74	12
Sweden (SE)	12,183	54	8346	51	3
Switzerland (CH)	10,257	70	5623	62	8
Australia (AU)	9822	41	7654	34	7
France (FR)	8945	76	6925	64	12
Belgium (BE)	7057	68	4806	63	5
Italy (IT)	6568	62	4056	58	4
Spain (ES)	6435	75	2340	61	14
Ireland (IE)	4193	41	3498	38	3
Brazil (BR)	3914	39	2899	32	7
Iceland (IS)	3868	13	158	13	0
India (IN)	3728	53	342	48	5
Luxembourg (LU)	3719	36	2224	33	3
Norway (NO)	3271	27	1374	26	1
Poland (PL)	3102	40	2505	34	6
Mexico (MX)	2908	48	1715	46	2
Portugal (PT)	2625	34	1370	31	3
Latvia (LV)	2391	21	761	20	1
Lithuania (LT)	2001	22	1052	21	1
Slovenia (SI)	1831	27	1543	20	7
Finland (FI)	1734	24	784	21	3
Turkey (TR)	1729	33	1126	32	1
Czech Republic (CZ)	1685	24	1339	22	2
United Arab Emirates (AE)	1581	21	80	21	0
Austria (AT)	1580	25	815	22	3
Singapore (SG)	1423	22	319	21	1

log frequency will be. For a better view, please check the HTML file in our Supporting Information. From **Fig. 6**, we can see that the N501Y mutation with a positive BFE change have a relatively high growth rate since early September 2020, which consist with the news that a new strain B.1.1.7 (also known as 20I/501Y.V1) in the United Kingdom has the potential to increase the pandemic trajectory [23]. Moreover, mutations V367F, E484K, N354D, and S373L with positive BFE changes also have a relatively higher mutation rate since early 2021, indicating that these four mutations may strengthen the binding of ACE2 and the S protein RBD, and potentially increase the infectivity of SARS-CoV-2. From **Fig. 5**, vaccine escape mutation E484K has dramatically disruptive effects on antibodies such as H11-H4, LY-CoV555, and DH1041.

Fig. 7 illustrates the log growth rate and log frequency of mutations on S protein RBD in the United States on a 10-day average. Similar to the United Kingdom, the VW mutation N501Y and VE mutation E484K recently have a high log growth rate. Additionally, ACE2 binding-strengthening mutations T385I, N439K, S477R, and L452R also have a high log growth rate since late 2020. To be noted, L452R is a VE mutation and HF mutation that had been reported as the key mutation that linked to COVID-19 outbreaks in California on January 17, 2021 [24].

Fig. 8 tracks the fast-growing mutations in Denmark. ACE2 binding-strengthening mutation L452R has a fast-growing tendency since December 8, 2020. From **Table 4**, mutation L452R may disrupt the binding of 28 existing antibodies with S protein. Binding-strengthening mutation S477N has a high growth rate from late July to early December. Mutation S477R that induce the positive BFE changes has a very rapid growth between November 28, 2020, to December 08, 2020, while the number of S447R mutations has recently not increased rapidly. To be noted, neither S477R nor S477N has much negative effect on the existing antibodies. The number of ACE2 binding-strengthening mutation N439K has kept a high growth rate since early August. However, the increasing rate of the N439K mutation slows down recently. As first reported in the United Kingdom, the N501Y mutation also has a fast-growing tendency since early December 2020, making the SARS-CoV-2 more infectious. A similar pattern can also be observed in Netherlands, Switzerland, Norway, and Sweden. Moreover, as shown in **Fig. 9**, four ACE2 binding-strengthening mutations have a rapid growth since late December 2020: N501Y, K417N, E484K, and P479S. Among them, K417N and E484K are both VE mutations with relatively high BFE changes, suggesting that researchers should keep tracking these mutations in the following months in Denmark. Furthermore, the B.1.351 lineage (also known as 20H/501Y.V2) was first identified in Nelson Mandela Bay, South Africa, which can be traced back to the beginning of October 2020, carries K417N, E484K, and N501Y on S protein RBD.

ACE2 binding-strengthening mutations in India include N440K, L452R, E484Q, N501Y, and E484K (see **Fig. 10**). It is worth to mention that except for N440K, all the ACE2 binding-strengthening mutations in India are either VE or VW mutations and have rapidly grown since February 06, 2021. Moreover, India variant B.1.617 has a 'double mutation' L452R and E484Q that are more infectious and vaccine evading, indicating that India's dire COVID-19 situation.

Singapore also has ACE2 binding-strengthening mutations K417N, E484K, N501Y, S477N, and L452R, as those found in other countries. Moreover, one ACE2 binding-strengthening mutation N440K with a high frequency has a relatively high growth rate since 2021 (See **Fig. 11**). Notably, the growth rate of mutation E484Q increases at the middle March of 2021. Considering the recent emergence of 'double mutation' L452R and E484Q in India, Singapore needs to pay more attention to tracking new variant B.1.617.

The National Institute of Infectious Diseases (NIID) in Japan first reported that four travelers from Brazil sampled a branch of the B.1.1.28 lineage called P.1 variant (also known as 20J/501Y.V3) [25]. This variant contains three mutations in the S protein RBD: VE mutation K417T, VE mutation E484K, and VW mutation N501Y. All of them are all ACE2 binding-strengthening mutations with a fast growth rate since late December 2020, as illustrated in **Fig. 12**.

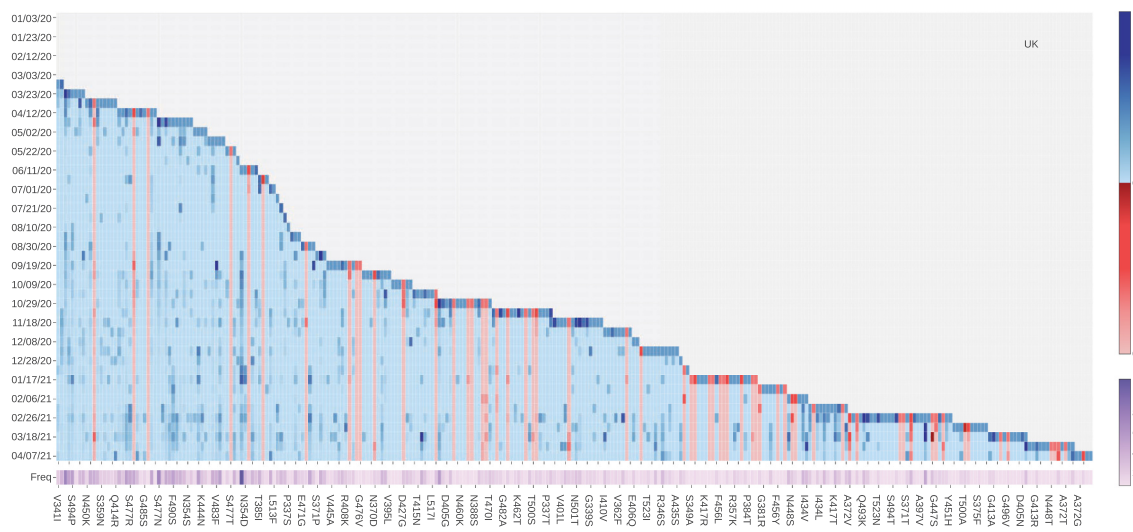


Fig. 6. The log growth rate and log frequency of mutations on S protein RBD in the United Kingdom. The blue and red colors respectively represent the binding-strengthening and binding-weakening mutations on RBD. The darker blue/red means the binding-strengthening/binding-weakening mutations with a higher growth rate in a specific 10-day period. The darker purple represents the mutation with a higher log frequency. (For interpretation of the references to colour in this figure legend, the reader is referred to the web version of this article.)

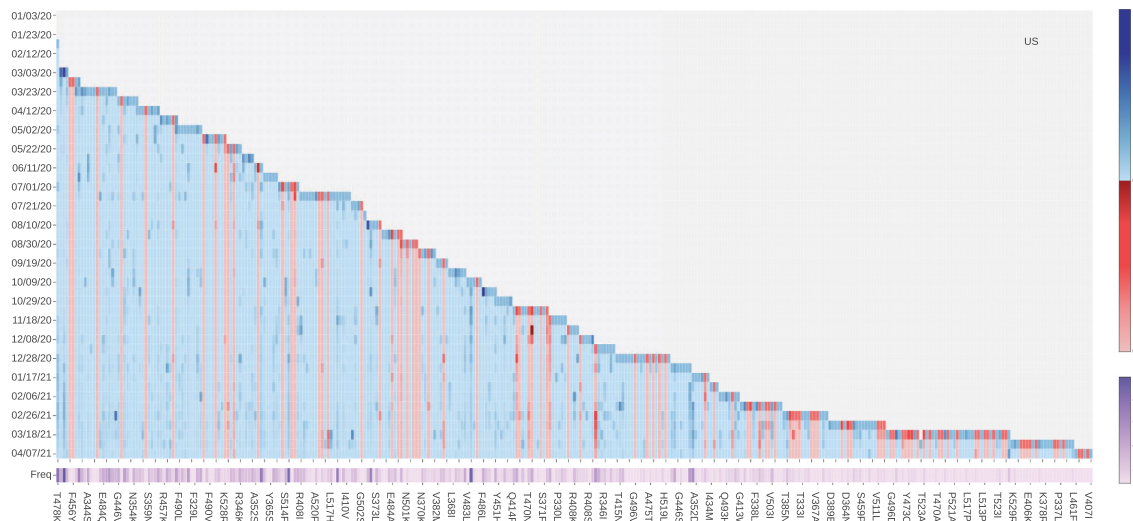


Fig. 7. The log growth rate and log frequency of mutations on S protein RBD in the United States. The blue and red colors respectively represent the binding-strengthening and binding-weakening mutations on RBD. The darker blue/red means the binding-strengthening/binding-weakening mutations with a higher growth rate in a specific 10-day period. The darker purple represents the mutation with a higher log frequency. (For interpretation of the references to colour in this figure legend, the reader is referred to the web version of this article.)

From analyzing the SNP profiles in Mexico, we notice that 6 ACE2 binding-strengthening mutations, L452R, S477N, T478K, S494P, E484K, and A552V, have a rapid growth since late October 2020. Among them, T478K is part of the Mexico variant B.1.1.222 and has the highest growth rate since late October 2020. Fig. 2 shows that T478K leads to the highest increase in ACE2-S protein RBD BFE change, indicating that fast-growing mutation T478K may potentially make the SARS-CoV-2 more transmissible and infectious. However, T478K does not pose a problem to antibodies.

2.5. Discussion

The BFE changes following 551 non-degenerate mutations on the S protein RBD are presented in Figs. S1–S5 of the Supporting information. These plots highlight the magnitude disparity in BFE changes induced by binding-strengthening mutations and binding-weakening mutations.

Such a large disparity indicates that SARS-CoV-2 is evolutionarily quite advance with respect to human infection. Figs. S6–S27 of the Supporting information provide the log growth rate and log frequency of mutations on S protein RBD in the Germany, Canada, Sweden, Switzerland, Australia, France, Belgium, Italy, Spain, Ireland, Iceland, Luxembourg, Norway, Poland, Portugal, Latvia, Lithuania, Slovenia, Finland, Turkey, Czechia, United Arab Emirates, and Austria. Table 6 shows the most significant mutations on S protein RBD of 31 countries with large sequencing data. This information, together with those given in Figs. 6–13, shows that, in addition to well-known mutations E484K, K417N, and N501Y, mutations N439K, L452R, S477N, S477R, and N501T are also ACE2 binding-strengthening mutations that have a high growth rate recently with high frequency. Tracking the growth rate tendency on a 10-day average for a long time enables us to detect the mutations that may strengthen the binding between S protein and ACE2, which will guide the development of vaccines and antibody therapies.

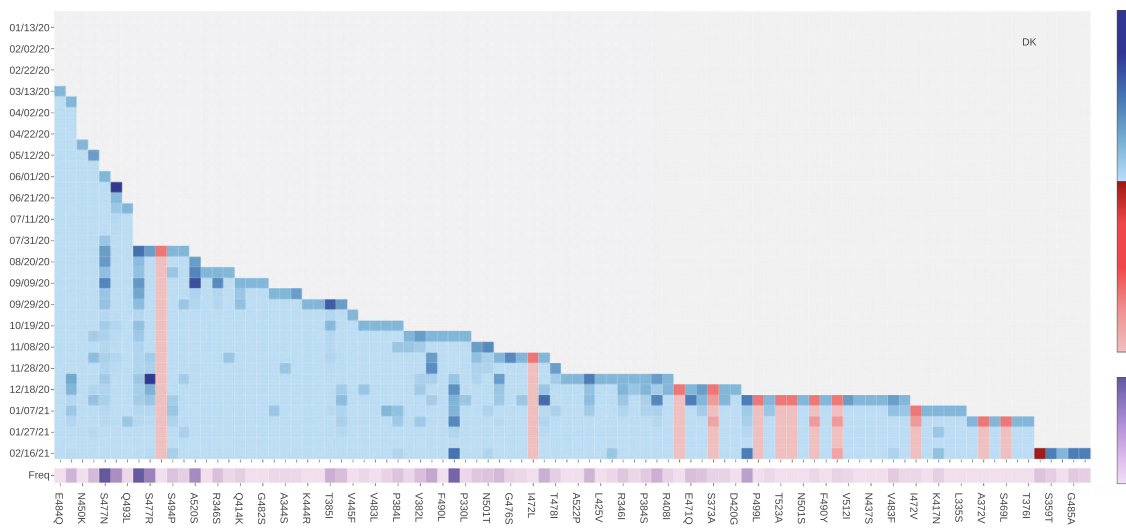


Fig. 8. The log growth rate and log frequency of mutations on S protein RBD in the Denmark. The blue and red colors respectively represent the binding-strengthening and binding-weakening mutations on RBD. The darker blue/red means the binding-strengthening/binding-weakening mutations with a higher growth rate in a specific 10-day period. The darker purple represents the mutation with a higher log frequency. (For interpretation of the references to colour in this figure legend, the reader is referred to the web version of this article.)

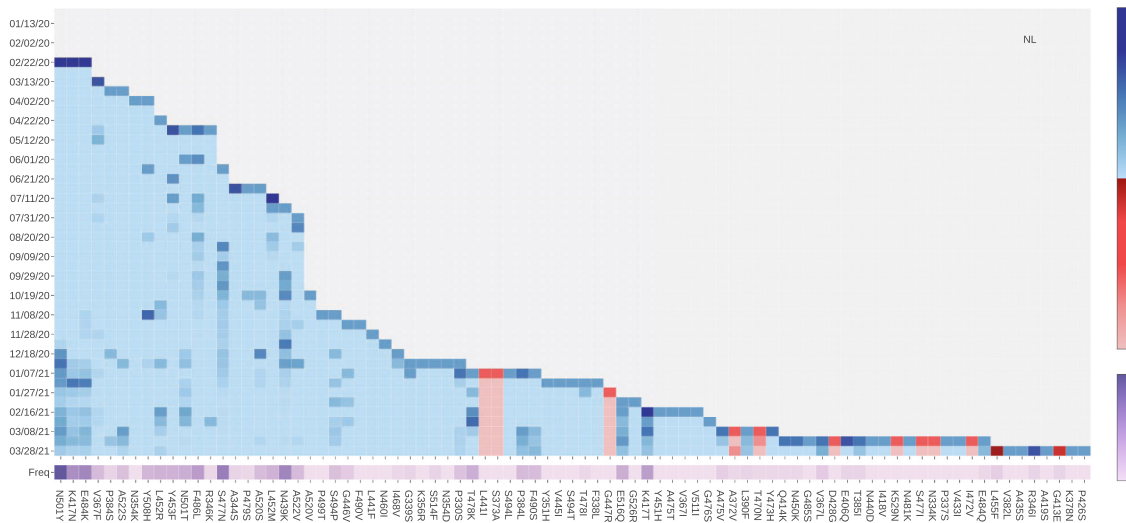


Fig. 9. The log growth rate and log frequency of mutations on S protein RBD in the Netherlands. The blue and red colors respectively represent the binding-strengthening and binding-weakening mutations on RBD. The darker blue/red means the binding-strengthening/binding-weakening mutations with a higher growth rate in a specific 10-day period. The darker purple represents the mutation with a higher log frequency. (For interpretation of the references to colour in this figure legend, the reader is referred to the web version of this article.)

Based on our study of mutation impacts on 106 antibodies [22], we found that the E484K mutation may cause a dramatically disruptive effect on antibodies such as H11-D4, P2B—2F6, Fab 2-4, H11-H4, COVA2-39, BD368-2, VH binder, S2M11, S2H13, CV07-270, P2C-1A3, P17, etc, which is consistent with the finding that E484K may affect neutralization by some polyclonal and monoclonal antibodies [26,27]. Mutation N501Y could weaken antibodies B38, A fab, CC12.1, VH binder, S309 S2H12 S304, C1A—B12, 910 30, STE90-C11, COVOX-150, COVOX-40, COVOX-88, and COVOX-269. Mutation N501T could weaken antibodies B38, CC12.1, S309 S2H12 S304, etc. Both E484 and N501 are coil residues on the RBD. Similarly, mutation K417N, which is a helix-residue of the RBD, could weaken antibodies B38, CB6, CV30, CC12.1, COVA2-04, BD-604, BD-236, A fab, P2C—1F11, C1A—B12, C1A—B3, C1A—F10, C1A—C2, etc. [22]. It is interesting to understand whether newly identified fast-growing mutations N439K, L452R, S477R, and E484K are also disruptive to vaccines and antibodies. By

checking the results reported early [22], we note that mutation L452R may make antibodies such as H11-D4, P2B—2F6, SR4, MR17, MR17-K99Y, H11-H4, BD-368-2, CV07-270, Fabs 298 52, CT-P59, etc., ineffective. However, mutation N439K is not as disruptive as E484K, K417N, N501Y, and N501T. It may weaken the binding of antibody SR4 and others. S477N can slightly weaken antibodies BD23 and CV07-250. Mutation S477R may even enhance the binding of most antibodies to the RBD. Finally, mutation E484Q may weaken the binding of many antibodies (such as LY-CoV555, DH1047, H11-H4, H11-D4, and CV07-270) in complex with S protein.

3. Methods

3.1. Data collection and pre-processing

The first complete SARS-CoV-2 genome sequence was released on the

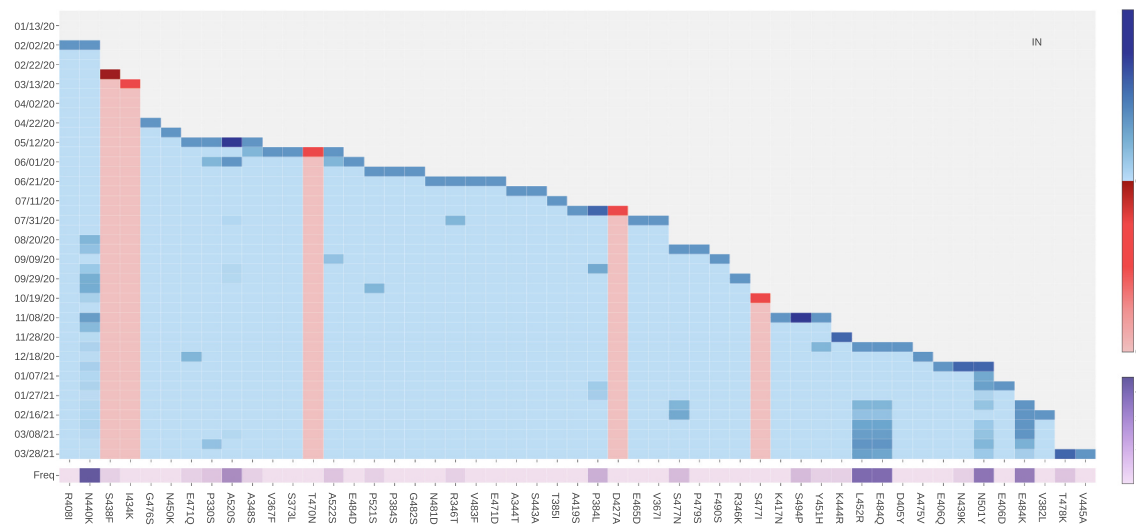


Fig. 10. The log growth rate and log frequency of mutations on S protein RBD in India. The blue and red colors respectively represent the binding-strengthening and binding-weakening mutations on RBD. The darker blue/red means the binding-strengthening/binding-weakening mutations with a higher growth rate in a specific 10-day period. The darker purple represents the mutation with a higher log frequency. (For interpretation of the references to colour in this figure legend, the reader is referred to the web version of this article.)

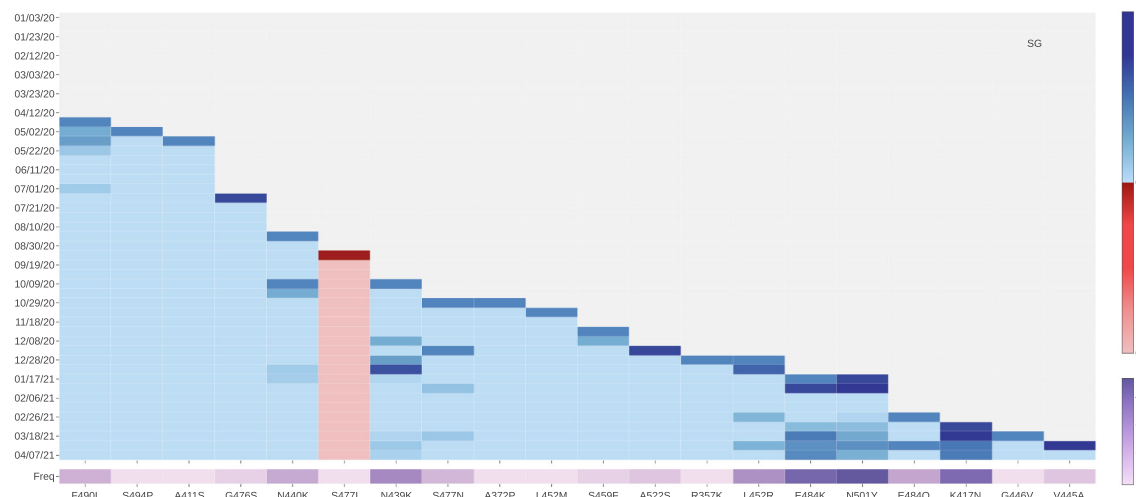


Fig. 11. The log growth rate and log frequency of mutations on S protein RBD in Singapore. The blue and red colors respectively represent the binding-strengthening and binding-weakening mutations on RBD. The darker blue/red means the binding-strengthening/binding-weakening mutations with a higher growth rate in a specific 10-day period. The darker purple represents the mutation with a higher log frequency. (For interpretation of the references to colour in this figure legend, the reader is referred to the web version of this article.)

GenBank (Access number: NC_045512.2) on January 5, 2020, by Zhang's group at Fudan University [28]. Since then, the rapid increment of the complete genome sequences is kept depositing to the GISAID database [29]. In this work, a total of 506,768 complete SARS-CoV-2 genome sequences with high coverage and exact submission date are downloaded from the GISAID database [29] (<https://www.gisaid.org/>) as of April 18, 2021. We take the NC_045512.2 as the reference genome, and the multiple sequence alignment (MSA) will be applied by Clustal Omega [30] with default parameters, which results in 506,768 SNP profiles. There are 106 antibodies or antibody combinations discussed with their corresponding PDB ID provided in the Supporting information.

3.2. The growth rate of mutations

Assume we have N SNP profiles, which have a total of M_n non-unique mutations and M_u unique mutations ($M_u \leq M_n$). Let ΔN_i be the number of

the increment of a particular mutation during the i th 10-day period, and N_i be the total number of a particular mutation.

Let the number of a particular mutation in the j th day of the i th 10-day period to be N_i^j , where $1 \leq i \leq 10$. Let the $\Delta N_i = N_i^{10} - N_i^1$ be the number of the increment of a particular mutation during the i th 10-day period. Then the growth rate of a particular mutation in the i th 10-day period will be defined as

$$R_i^j = \begin{cases} 0, & \text{if } \Delta N_i = 0 \text{ and } \sum_{k=1}^{i-1} \Delta N_k = 0, \\ \frac{\Delta N_i}{(1 + \sum_{k=1}^{i-1} \Delta N_k)}, & \text{else.} \end{cases} \quad (1)$$

Moreover, the natural logarithm growth rate of a particular mutation in the i th 10-day period will be defined as

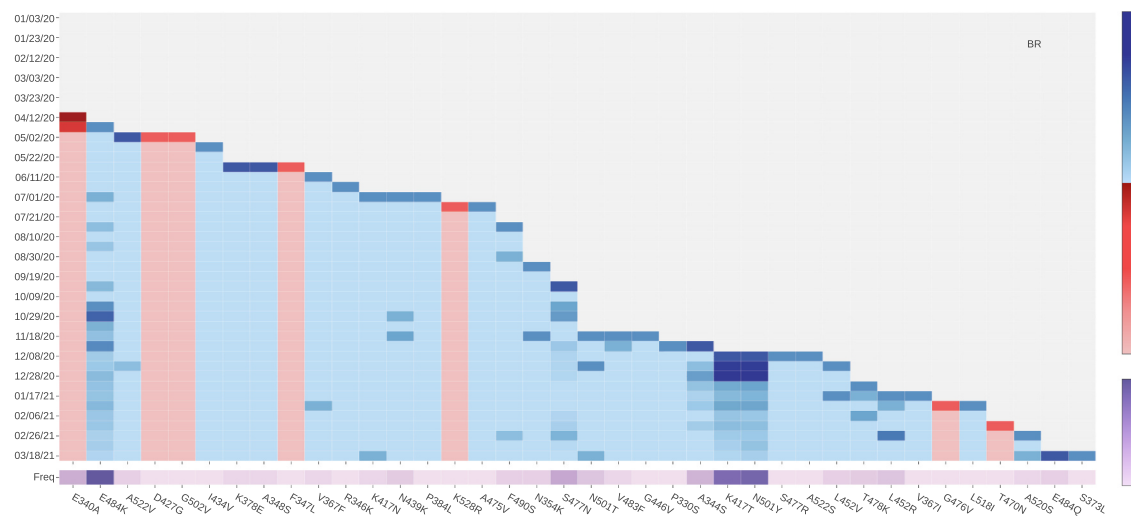


Fig. 12. The log growth rate and log frequency of mutations on S protein RBD in Brazil. The blue and red colors respectively represent the binding-strengthening and binding-weakening mutations on RBD. The darker blue/red means the binding-strengthening/binding-weakening mutations with a higher growth rate in a specific 10-day period. The darker purple represents the mutation with a higher log frequency. (For interpretation of the references to colour in this figure legend, the reader is referred to the web version of this article.)

Table 6
Most significant mutations on S protein RBD of 31 countries with large sequencing data.

Country	Most significant mutations
United Kingdom	N439K, S477N, S494P, and N501Y,
United States	A520S, N501Y, S494P, E484K, S477N, N501T, and L452R
Denmark	S477N, Y453F, S477R, N439K, and N501Y
Germany	N439K, S477N, and N501Y
Canada	R357K, E484K, and L452R
Netherlands	N501Y, K417N, E484K, F486L, S477N, N439K, and K417T
Sweden	E484K, S477N, N439K, N501Y, and K417N
Switzerland	N439K, S477N, N501Y, Q414K, N450K, L452R, and T478K
Australia	S477N, N501Y, L452R, L455F, N439K, and N501T
France	S477N, N439K, L452R, A522S, E484K, N501Y, and K417T
Belgium	N501Y, S477N, E484K, N450K, K417N, and K417T
Italy	N439K, S477N, L452R, E484K, N501Y, K417T, N440K, and Q414K
Spain	S477N, N501Y, S494P, and E484K
Ireland	N439K, N501Y, and E484K
Brazil	E484K, K417T, and N501Y
Iceland	S477N, N439K, and E406Q
India	N440K, A520S, P384L, S477N, S494P, L452R, E484Q, N501Y, and E484K
Luxembourg	S477N, N439K, and N501Y
Norway	N439K, S477N, A520S, and N501Y
Poland	N439K, S477N, A522S, N501Y, F494P
Mexico	L452R and T478K
Portugal	S477N, L452R, and N501Y
Latvia	E484K, N501Y, N439K, V367F, A522V, S494P, and K417N
Lithuania	V362F, N439K, N501Y, S477N, S490L, L452R, S477I, and E471Q
Slovenia	N439K, S477R, S477N, N501Y, K356R, and E484K
Finland	P384L, S477N, N439K, A352S, and N501Y
Turkey	S477N, N501Y, K417N, N501T, and E484K
Czech Republic	S459Y, N439K, S477N, N501Y, E484K, and K417N
United Arab Emirates	N501Y, N440K, S477N, N439K, E484K, and K417N
Austria	S477N, N439K and N501Y
Singapore	F490L, N440K, N439K, S477N, L452R, E484K, N501Y, and K417N

$$LR_j^i = \log(R_j^i + 1) \quad (2)$$

3.3. TopNetTree model for protein-protein interaction (PPI) binding free energy changes upon mutation

Mutation-induced protein-protein binding free energy (BFE) changes are an important approach for understanding the impact of mutations on protein-protein interactions (PPIs) and viral infectivity [31]. A variety of advanced methods has been developed [31,32]. The topology-based network tree (TopNetTree) model [15,21] is applied to predict mutation-induced BFE changes of PPIs in this work. TopNetTree model was implemented by integrating the topological representation and network tree (NetTree) to predict the BFE changes ($\Delta\Delta G$) of PPIs following mutations [21]. The structural complexity of protein-protein complexes is simplified by algebraic topology [33–35] and is represented as the vital biological information in terms of topological invariants. NetTree integrates the advantages of convolutional neural networks (CNN) and gradient-boosting trees (GBT), such that CNN is treated as an intermediate model that converts vectorized element- and site-specific persistent homology features into a higher-level abstract feature, and GBT uses the upstream features and other biochemistry features for prediction. The performance test of tenfold cross-validation on the dataset (SKEMPI 2.0 [36]) was carried out using gradient boosted regression tree (GBRTs). The errors with the SKEMPI 2.0 dataset are 0.85 in terms of Pearson correlation coefficient (R_p) and 1.11 kcal/mol in terms of the root mean square error (RMSE) [21].

3.3.1. Training sets for TopNetTree model

The TopNetTree model is trained by several important training sets. The most important dataset which provides the information for BFE changes upon mutations in the SKEMPI 2.0 dataset [36]. The SKEMPI 2.0 is an updated version of the SKEMPI database, which contains new mutations and data from other three databases: AB-Bind [37], PROXIMATE [38], and dbMPIKT [39]. There are 7085 elements including single- and multi-point mutations in SKEMPI 2.0. 4169 variants in 319 different protein complexes are filtered as single-point mutations are used for TopNetTree model training. Moreover, SARS-CoV-2 related datasets are also included to improve the prediction accuracy after a label transformation. They are all deep mutation enrichment ratio data, mutational scanning data of ACE2 binding to the receptor-binding domain (RBD) of the S protein (including 2223 training samples) [40],

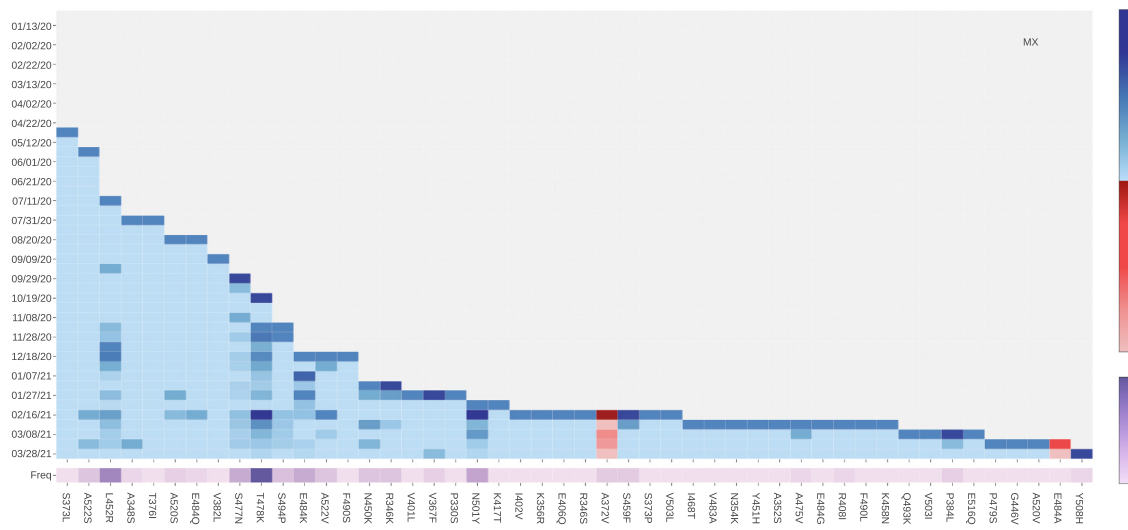


Fig. 13. The log growth rate and log frequency of mutations on S protein RBD in Mexico. The blue and red colors respectively represent the binding-strengthening and binding-weakening mutations on RBD. The darker blue/red means the binding-strengthening/binding-weakening mutations with a higher growth rate in a specific 10-day period. The darker purple represents the mutation with a higher log frequency. (For interpretation of the references to colour in this figure legend, the reader is referred to the web version of this article.)

mutational scanning data of RBD binding to ACE2 (including 3783 and 1539 training samples, respectively) [41,42], and mutational scanning data of RBD binding to CTC-445.2 and of CTC-445.2 binding to the RBD (including 1539 and 2831 training samples, respectively) [42]. The validation results for this SARS-CoV-2 TopNetTree model on SARS-CoV-2 related test set can be found in the literature [22].

3.3.2. Topology-based feature generation of PPIs

Persistent homology, a branch of algebraic topology, is a powerful method for simplifying the structural complexity of macromolecules [33–35]. To construct topological data analysis on protein-protein interactions, we first preset the constructions for a PPI complex into various subsets.

1. \mathcal{A}_m : atoms of the mutation sites.
2. $\mathcal{A}_{mn}(r)$: atoms in the neighborhood of the mutation site within a cut-off distance r .
3. $\mathcal{A}_{Ab}(r)$: antibody atoms within r of the binding site.
4. $\mathcal{A}_{Ag}(r)$: antigen atoms within r of the binding site.
5. $\mathcal{A}_{ele}(E)$: atoms in the system that has atoms of element type E . The distance matrix is specially designed such that it excludes the interactions between the atoms form the same set. For interactions between atoms a_i and a_j in set \mathcal{A} and/or set \mathcal{B} , the modified distance is defined as

$$D_{\text{mod}}(a_i, a_j) = \begin{cases} \infty, & \text{if } a_i, a_j \in \mathcal{A}, \text{ or } a_i, a_j \in \mathcal{B}, \\ D_e(a_i, a_j), & \text{if } a_i \in \mathcal{A} \text{ and } a_j \in \mathcal{B}, \end{cases} \quad (3)$$

where $D_e(a_i, a_j)$ is the Euclidian distance between a_i and a_j .

In algebraic topology, different molecular atoms can be constructed as points presented by $v_0, v_1, v_2, \dots, v_k$ as $k + 1$ affinely independent points in simplicial complex. A simplicial complex is a finite collection of sets of points $K = \{\sigma_i\}$, and σ_i are called linear combinations of these points in \mathbb{R}^n ($n \geq k$). To construct a simplicial complex, the Vietoris-Rips (VR) complex and alpha complex, which are widely used for point clouds, are applied in this model [34]. The boundary operator for a k -simplex would transfer a k -simplex to a $k - 1$ -simplex. Consequently, the algebraic construction to connect a sequence of complexes by boundary maps is called a chain complex

$$\dots \xrightarrow{\partial_{i+1}} C_i(X) \xrightarrow{\partial_i} C_{i-1}(X) \xrightarrow{\partial_{i-1}} \dots \xrightarrow{\partial_2} C_1(X) \xrightarrow{\partial_1} C_0(X) \xrightarrow{\partial_0} 0$$

and the k th homology group is the quotient group defined by

$$H_k = Z_k / B_k. \quad (4)$$

Then the Betti numbers are defined by the ranks of k th homology group H_k which counts k -dimensional invariants, especially, $\beta_0 = \text{rank}(H_0)$ reflects the number of connected components, $\beta_1 = \text{rank}(H_1)$ reflects the number of loops, and $\beta_2 = \text{rank}(H_2)$ reveals the number of voids or cavities. Together, the set of Betti numbers $\{\beta_0, \beta_1, \beta_2, \dots\}$ indicates the intrinsic topological property of a system.

Persistent homology is devised to track the multiscale topological information over different scales along a filtration [34] and is significantly important for constructing feature vectors for the machine learning method. Features generated by binned barcode vectorization can reflect the strength of atom bonds, van der Waals interactions, and can be easily incorporated into a CNN, which captures and discriminates local patterns. Another method of vectorization is to get the statistics of bar lengths, birth values, and death values, such as sum, maximum, minimum, mean, and standard derivation. This method is applied to vectorize Betti-1 (H_1) and Betti-2 (H_2) barcodes obtained from alpha complex filtration based on the fact that higher-dimensional barcodes are sparser than H_0 barcodes.

3.3.3. Machine learning models

It is very challenging to predict binding affinity changes following mutation for PPIs due to the complex dataset and 3D structures. A hybrid machine learning algorithm that integrates a CNN and GBT is designed to overcome difficulties, such that partial topologically simplified descriptions are converted into concise features by the CNN module and a GBT module is trained on the whole feature set for a robust predictor with effective control of overfitting [21]. The gradient boosting tree (GBT) method produces a prediction model as an ensemble method which is a class of machine learning algorithms. It builds a popular module for regression and classification problems from weak learners. By the assumption that the individual learners are likely to make different mistakes, the method using a summation of the weak learners to eliminate the overall error. Furthermore, a decision tree is added to the ensemble depending on the current prediction error on the training dataset. Therefore, this method (a topology-based GBT or TopGBT) is relatively robust against hyperparameter tuning and overfitting, especially for a moderate number of features. The GBT is shown for its robustness against overfitting, good performance for moderately small

data sizes, and model interpretability. The current work uses the package provided by scikit-learn (v 0.23.0) [43]. A supervised CNN model with the PPI $\Delta\Delta G$ as labels is trained for extracting high-level features from H_0 barcodes. Once the model is set up, the flatten layer neural outputs of CNN are feed into a GBT model to rank their importance. Based on the importance, an ordered subset of CNN-trained features is combined with features constructed from high-dimensional topological barcodes, H_1 and H_2 into the final GBT model.

4. Conclusion

Understanding the evolution trend of severe acute respiratory syndrome coronavirus 2 (SARS-CoV-2) and estimating its threats to the existing vaccines and antibody drugs are of paramount importance to the current battle against coronavirus disease 2019 (COVID-19). To this end, we carry out a unique analysis of mutations on the spike (S) protein receptor-binding domain (RBD). Our study is based on comprehensive 506,768 SARS-CoV-2 genome isolates recorded on the Mutation Tracker (https://users.math.msu.edu/users/weig/SARS-CoV-2_Mutation_Tracker.html). There are 6945 unique single mutations and 2,194,305 non-unique mutations on the S protein gene. Therefore, an average genome sample has 2.6 mutations on the S protein but new samples have increasingly more mutations. In terms of the protein sequence, 651 non-degenerate mutations occurred on the RBD. However, most of these RBD mutations have a relatively low frequency, leaving 100 most observed mutations that have been detected more than 28 times in the database. We track fast-growing (FG) RBD mutations in 31 pandemic-devastated countries, including the UK, the US, Singapore, Spain, India, Brazil, etc. To avoid random low-frequency mutations, we pursue this task by analyzing the 10-day growth rate of 100 most observed RBD mutations. We show that four fast-growing mutations N439K, S477N, S477R, and N501T in addition to all known infectious variants containing N501Y, L452R, E484Q, E484K, and K417N, deserve the world's attention.

Additionally, we reveal that essentially all the 100 most observed mutations on the RBD strengthen the RBD binding with the host angiotensin-converting enzyme 2 (ACE2), based on a cutting-edge topology-based neural network tree (TopNetTree) model trained on SARS-CoV-2 experimental datasets [21,22]. More specifically, we found that mutations N501Y, E484K, and K417N in the United Kingdom (UK), South Africa, or Brazil variants, L452R and E484Q in the India, as well as mutations N439K, S477N, S477R, and N501T are all associated with the enhancement of the BFE of the S protein and ACE2, confirming the earlier speculation. This result suggests that SARS-CoV-2 has evolved into more infectious strains due to the wide-spread transmission.

Finally, the early finding shows that more 70% mutations would weaken the efficacy of known antibodies [22]. We report that rapidly growing mutations S494P, Q493L, K417N, F486L, F490S, R403K, E484K, K417T, L452R, E484Q, A475S, and F490L are more likely to disrupt existing vaccines and many antibody drugs. While mutations Q493R, R408I, Q493H, P384S, and N501T can also be disruptive, but mutations N439K, V367F, and S477R are not as disruptive as other rapidly growing ones. Note that L452R in the California variant B.1.427 is as infectious as N501Y and as disruptive as E484K. We have predicted vaccine escape mutations that are not only fast-growing but also can disrupt many existing vaccines. We have also identified vaccine weakening mutations as fast-growing RBD mutations that will weaken the binding between the S protein and many existing antibodies. A list of vaccine escape and vaccine weakening RBD mutations is predicted. We unveil that regulated by host gene editing, viral proofreading, random genetic drift, and natural selection, the mutations on the S protein RBD tend to disrupt the existing antibodies and vaccines and increase the transmission and infectivity of SARS-CoV-2.

Data and model availability

The SARS-CoV-2 SNP data in the world is available at Mutation

Tracker. The information of 106 antibodies with their corresponding PDB IDs can be found in the Section S2 of the Supporting information. The SARS-CoV-2 S protein RBD SNP data in 31 countries can be downloaded from the Supplementary data. The TopNetTree model is available at TopNetTree. The related training datasets are described in Section 3.3.3.

Acknowledgment

This work was supported in part by NIH grant GM126189, NSF grants DMS-2052983, DMS-1761320, and IIS-1900473, NASA grant 80NSSC21M0023, Michigan Economic Development Corporation, George Mason University award PD45722, Bristol-Myers Squibb 65109, and Pfizer. The authors thank The IBM TJ Watson Research Center, The COVID-19 High Performance Computing Consortium, NVIDIA, and MSU HPCC for computational assistance. RW thanks Dr. Changchuan Yin for useful discussion.

Appendix A. Supplementary data

Supplementary data to this article can be found online at <https://doi.org/10.1016/j.ygeno.2021.05.006>.

References

- [1] Christian Jean Michel, Claudine Mayer, Olivier Poch, Julie Dawn Thompson, Characterization of accessory genes in coronavirus genomes, 2020.
- [2] Yosra A. Helmy, Mohamed Fawzy, Ahmed Elaswad, Ahmed Sobieh, Scott P. Kenney, Awad A. Shehata, The covid-19 pandemic: a comprehensive review of taxonomy, genetics, epidemiology, diagnosis, treatment, and control, *J. Clin. Med.* 9 (4) (2020) 1225.
- [3] Ahmad Abu Turab Naqvi, Kisa Fatima, Taj Mohammad, Urooj Fatima, Indrakant K. Singh, Archana Singh, Shaikh Muhammad Atif, Gururao Hariprasad, Gulam Mustafa Hasan, Md Imtaiyaz Hassan, Insights into sars-cov-2 genome, structure, evolution, pathogenesis and therapies: structural genomics approach, *Biochim. Biophys. Acta (BBA) Mol. Bas. Dis.* (2020) 165878.
- [4] Mu Jingfang, Yaohui Fang, Qi Yang, Ting Shu, An Wang, Muhan Huang, Jin Liang, Fei Deng, Qiu Yang, Xi Zhou, Sars-cov-2 n protein antagonizes type i interferon signaling by suppressing phosphorylation and nuclear translocation of stat1 and stat2, *Cell Discov.* 6 (1) (2020) 1–4.
- [5] Markus Hoffmann, Hannah Kleine-Weber, Simon Schroeder, Nadine Krüger, Tanja Herrler, Sandra Erichsen, Tobias S. Schiergens, Georg Herrler, Nai-Huei Wu, Andreas Nitsche, et al., SARS-CoV-2 cell entry depends on ACE2 and TMPRSS2 and is blocked by a clinically proven protease inhibitor, *Cell* 181 (2020) 271–280.e8.
- [6] Marion Sevajol, Lorenzo Subissi, Etienne Decroly, Bruno Canard, Isabelle Imbert, Insights into RNA synthesis, capping, and proofreading mechanisms of SARS-coronavirus, *Virus Res.* 194 (2014) 90–99.
- [7] François Ferron, Lorenzo Subissi, Ana Theresa Silveira De Moraes, Nhung Thi Tuyet Le, Marion Sevajol, Laure Gluais, Etienne Decroly, Clemens Vonrhein, Gérard Bricogne, Bruno Canard, et al., Structural and molecular basis of mismatch correction and ribavirin excision from coronavirus RNA, *Proc. Natl. Acad. Sci.* 115 (2) (2018), E162–E171.
- [8] Rui Wang, Yuta Hozumi, Yong-Hui Zheng, Changchuan Yin, Guo-Wei Wei, Host immune response driving SARS-CoV-2 evolution, *Viruses* 12 (10) (2020) 1095.
- [9] Rafael Sanjuán, Pilar Domingo-Calap, Mechanisms of viral mutation, *Cell. Mol. Life Sci.* 73 (23) (2016) 4433–4448.
- [10] Nathan D. Grubaugh, William P. Hanage, Angela L. Rasmussen, Making sense of mutation: what D614G means for the COVID-19 pandemic remains unclear, *Cell* 182 (4) (2020) 794–795.
- [11] Wendong Li, Zhengli Shi, Meng Yu, Wuze Ren, Craig Smith, Jonathan H. Epstein, Hanzhong Wang, Gary Cramer, Zhihong Hu, Huaqun Zhang, et al., Bats are natural reservoirs of SARS-like coronaviruses, *Science* 310 (5748) (2005) 676–679.
- [12] Qu Xia-Xia, Pei Hao, Xi-Jun Song, Si-Ming Jiang, Yan-Xia Liu, Pei-Gang Wang, Xi Rao, Huai-Dong Song, Sheng-Yue Wang, Yu Zuo, et al., Identification of two critical amino acid residues of the severe acute respiratory syndrome coronavirus spike protein for its variation in zoonotic tropism transition via a double substitution strategy, *J. Biol. Chem.* 280 (33) (2005) 29588–29595.
- [13] Huai-Dong Song, Tu Chang-Chun, Guo-Wei Zhang, Sheng-Yue Wang, Kui Zheng, Lian-Cheng Lei, Qiu-Xia Chen, Yu-Wei Gao, Hui-Qiong Zhou, Hua Xiang, et al., Cross-host evolution of severe acute respiratory syndrome coronavirus in palm civet and human, *Proc. Natl. Acad. Sci.* 102 (7) (2005) 2430–2435.
- [14] Alexandra C. Walls, Young-Jun Park, M. Alejandra Tortorici, Abigail Wall, Andrew T. McGuire, Yael Veesler, Structure, function, and antigenicity of the SARS-CoV-2 spike glycoprotein, *Cell* 181 (2020) 281–292.
- [15] Jiahui Chen, Rui Wang, Menglin Wang, Guo-Wei Wei, Mutations strengthened SARS-CoV-2 infectivity, *J. Mol. Biol.* 432 (2020) 5212–5226.

[16] Rui Wang, Jiahui Chen, Yuta Hozumi, Changchuan Yin, Guo-Wei Wei, Decoding asymptomatic covid-19 infection and transmission, *J. Phys. Chem. Lett.* 11 (23) (2020) 10007–10015.

[17] Julian W. Tang, Paul A. Tambyah, David S.C. Hui, Emergence of a new SARS-CoV-2 variant in the UK, *J. Infect.* 82 (2020) E27–E28.

[18] Mulenga Mwenda, Ngonda Saasa, Nyambe Sinyange, George Busby, Peter J Chipimo, Jason Hendry, Otridah Kapona, Samuel Yingst, Jonas Z Hines, Peter Minchella, et al. Detection of b. 1.351 sars-cov-2 variant—zambia, december 2020. 2021.

[19] Nuno R. Faria, Ingra Morales Claro, Darlan Candido, L.A. Moyses Franco, Pamela S. Andrade, Thais M. Coletti, Camila A.M. Silva, Flavia C. Sales, Erika R. Manuli, Renato S. Aguilar, et al., Genomic characterisation of an emergent SARS-CoV-2 lineage in Manaus: preliminary findings, *Virological* (2021). <https://www.icpcovid.com/sites/default/files/2021-01/Ep%20102-1%20Genomic%20characterisation%20of%20an%20emergent%20SARS-CoV-2%20lineage%20in%20Manaus%20Genomic%20Epidemiology%20-%20Virological.pdf>.

[20] Sarah Cherian, Varsha Potdar, Santosh Jadhav, Pragya Yadav, Nivedita Gupta, Mousmi Das, Soumitra Das, Anurag Agarwal, Sujeeet Singh, Priya Abraham, et al., Convergent evolution of SARS-CoV-2 spike mutations, L452R, E484Q and P681R, in the second wave of COVID-19 in Maharashtra, India, *bioRxiv* (2021), <https://doi.org/10.1101/2021.04.22.440932>.

[21] Menglun Wang, Zixuan Cang, Guo-Wei Wei, A topology-based network tree for the prediction of protein–protein binding affinity changes following mutation, *Nat. Machine Intellig.* 2 (2) (2020) 116–123.

[22] Jiahui Chen, Kaifu Gao, Rui Wang, Guo-Wei Wei, Prediction and mitigation of mutation threats to COVID-19 vaccines and antibody therapies, *Chem. Sci.* (2021), <https://doi.org/10.1039/D1SC01203G> (in press).

[23] Summer E. Galloway, Prabasaj Paul, Duncan R. MacCannell, Michael A. Johansson, John T. Brooks, Adam MacNeil, Rachel B. Slayton, Suxiang Tong, Benjamin J. Silk, Gregory L. Armstrong, et al., Emergence of sars-cov-2 b. 1.1. 7 lineage—united states, december 29, 2020–january 12, 2021, *Morbid. Mort. Weekly Rep.* 70 (3) (2021) 95.

[24] Wenjuan Zhang, Brian Davis, Stephanie S. Chen, Jorge Sincuir Martinez, Jasmine T. Plummer, Eric Vail, Emergence of a Novel SARS-CoV-2 Variant in Southern California, *JAMA* 325 (13) (2021) 1324–1326, <https://doi.org/10.1001/jama.2021.1612>.

[25] Felipe Naveca, Cristiano da Costa, Valdinei Nascimento, Victor Souza, André Corado, Fernanda Nascimento, Ágatha Costa, Débora Duarte, George Silva, Matilde Meja, et al. Sars-cov-2 reinfection by the new variant of concern (voc) p. 1 in amazonas, brazil. *virological. org*. Preprint available at: <https://virological.org/g/t/sars-cov-2-reinfection-by-the-new-variant-of-concern-voc-p-1-in-amazonas-brasil/596>. Available at: <https://virological.org/t/sars-cov-2-reinfection-by-the-new-variant-of-concern-voc-p-1-in-amazonas-brazil/596>, 2021.

[26] Yiska Weisblum, Fabian Schmidt, Fengwen Zhang, Justin DaSilva, Daniel Poston, Julio C.C. Lorenzi, Frauke Muecksch, Magdalena Rutkowska, Hans-Heinrich Hoffmann, Eleftherios Michailidis, et al., Escape from neutralizing antibodies by sars-cov-2 spike protein variants, *Elife* 9 (2020), e61312.

[27] Paola Cristina Resende, João Felipe Bezerra, Romero Henrique Teixeira de Vasconcelos, Igor Arantes, Luciana Appolinario, Ana Carolina Mendonça, Anna Carolina Paixão, Ana Carolina Duarte Rodrigues, Thauane Silva, Alice Sampaio Rocha, et al. Spike e484k mutation in the first sars-cov-2 reinfection case confirmed in Brazil, 2020. January, 10:2021, 2021.

[28] Fan Wu, Su Zhao, Bin Yu, Yan-Mei Chen, Wen Wang, Zhi-Gang Song, Yi Hu, Zhao-Wu Tao, Jun-Hua Tian, Yuan-Yuan Pei, et al., A new coronavirus associated with human respiratory disease in China, *Nature* 579 (7798) (2020) 265–269.

[29] Yuelong Shu, John McCauley, GISAID: global initiative on sharing all influenza data—from vision to reality, *Eurosurveillance* 22 (13) (2017).

[30] Fabian Sievers, Desmond G. Higgins, Clustal omega, accurate alignment of very large numbers of sequences, in: *Multiple Sequence Alignment Methods*, Springer, 2014, pp. 105–116.

[31] Gen Li, Swagata Pahari, Adithya Krishna Murthy, Siqi Liang, Robert Fragoza, Haiyuan Yu, Emil Alexov, SAAMBE-SEQ: a sequence-based method for predicting mutation effect on protein–protein binding affinity, *Bioinformatics* (2020), <https://doi.org/10.1093/bioinformatics/btaa761>.

[32] Carlos H.M. Rodrigues, Yoochan Myung, Douglas E.V. Pires, David B. Ascher, mcsim-ppi2: predicting the effects of mutations on protein–protein interactions, *Nucleic Acids Res.* 47 (W1) (2019) W338–W344.

[33] Gunnar Carlsson, Topology and data, *Bull. Am. Math. Soc.* 46 (2) (2009) 255–308.

[34] Herbert Edelsbrunner, David Letscher, Afra Zomorodian, Topological persistence and simplification, in: *Proceedings 41st Annual Symposium on Foundations of Computer Science*, IEEE, 2000, pp. 454–463.

[35] Kelin Xia, Guo-Wei Wei, Persistent homology analysis of protein structure, flexibility, and folding, *Int. J. Numer. Meth. Biomed. Eng.* 30 (8) (2014) 814–844.

[36] Justina Jankauskaité, Brian Jiménez-García, Justas Dapkūnas, Juan Fernández-Rocío, Iain H. Moal, Skempi 2.0: an updated benchmark of changes in protein–protein binding energy, kinetics and thermodynamics upon mutation, *Bioinformatics* 35 (3) (2019) 462–469.

[37] Sarah Sirin, James R. Apgar, Eric M. Bennett, Amy E. Keating, AB-Bind: antibody binding mutational database for computational affinity predictions, *Protein Sci.* 25 (2) (2016) 393–409.

[38] Sherlyn Jemimah, K. Yugandhar, M. Michael Gromiha, Proximate: a database of mutant protein–protein complex thermodynamics and kinetics, *Bioinformatics* 33 (17) (2017) 2787–2788.

[39] Quanya Liu, Peng Chen, Bing Wang, Jun Zhang, Jinyan Li, dbmpkt: a database of kinetic and thermodynamic mutant protein interactions, *BMC Bioinform.* 19 (1) (2018) 1–7.

[40] Erik Procko. The sequence of human ace2 is suboptimal for binding the s spike protein of sars coronavirus 2. *BioRxiv*, 2020.

[41] Tyler N. Starr, Allison J. Greaney, Sarah K. Hilton, Daniel Ellis, Katharine H. D. Crawford, Adam S. Dingens, Mary Jane Navarro, John E. Bowen, M. Alejandra Tortorici, Alexandra C. Walls, et al., Deep mutational scanning of sars-cov-2 receptor binding domain reveals constraints on folding and ace2 binding, *Cell* 182 (5) (2020) 1295–1310.

[42] Thomas W. Linsky, Renan Vergara, Nuria Codina, Jorgen W. Nelson, Matthew J. Walker, Wen Su, Christopher O. Barnes, Tien-Ying Hsiang, Katharina Esser-Nobis, Kevin Yu, et al., De novo design of potent and resilient ace2 decoys to neutralize sars-cov-2, *Science* 370 (6521) (2020) 1208–1214.

[43] Fabian Pedregosa, Gaël Varoquaux, Alexandre Gramfort, Vincent Michel, Bertrand Thirion, Olivier Grisel, Mathieu Blondel, Peter Prettenhofer, Ron Weiss, Vincent Dubourg, et al., Scikit-learn: machine learning in python, *J. Mach. Learn. Res.* 12 (2011) 2825–2830.